Flow and Transport in regions with Aquatic Vegetation

Heidi M. Nepf
Department of Civil and Environmental Engineering
Massachusetts Institute of Technology
Cambridge, MA 02139, USA
hmnepf@mit.edu

Running Title: Flow near Aquatic Vegetation

Corresponding Author: Heidi M. Nepf
Department of Civil and Environmental Engineering
Massachusetts Institute of Technology
77 Massachusetts Avenue
Building 48-216D
Cambridge, MA 02139, USA
hmnepf@mit.edu
(617)-253-8622

Key Words:

Aquatic Vegetation

Canopy

Canopy Shear-Layer

Monami

Turbulence

Turbulent Transport

Key Terms/Definitions

Emergent Vegetation =	rooted vegetation that penetrates the free surface and thus occupies the full water depth
Submerged Vegetation =	rooted vegetation with a vertical extent less than the water depth
Canopy Shear Layer =	the region of velocity shear generated by the drag discontinuity at top of submerged canopy
Canopy-Scale Turbulence =	vortices generated within canopy-shear-layer by Kelvin-Helmholtz instability.
Stem-Scale Turbulence =	turbulence generated in the wakes of individual stems and branches

Sidebar: Waves over Submerged Canopies

Because the flow beneath waves is unsteady, inertial forces can be comparable to or larger than canopy drag at high wave frequencies, including typical wind-wave frequencies. For these conditions, the wave velocity is not significantly damped within the canopy, in contrast to the large degree of damping observed for dense canopies in uni-directional flow (Figure 3). Further, in analogy to viscous boundary streaming, canopy drag induces a non-zero wave stress, which in turn generates a mean mass-drift within the canopy. Steady currents with magnitudes up to 40% of the near-bed orbital velocity have been measured in model canopies.

Lowe R, Koseff J, Monismith S. 2005. Oscillatory flow through submerged canopies: 1. Velocity structure. *J. Geophys. Res.,* 110*,* C10016, doi:10.1029/2004JC002788

Luhar M, Coutu S, Infantes E, Fox S, Nepf H. 2010. Wave induced velocities inside a model seagrass bed. *J.Geophys. Res.* 115*,* C12005*,* doi:10.1029/2010JC006345

Abstract:

This paper describes mean and turbulent flow and mass transport in the presence of aquatic vegetation. Within emergent canopies, the turbulent length-scales are set by the stem diameter and spacing, and the mean flow is determined by the distribution of canopy frontal area. Sparse submerged canopies enhance bed roughness and near-bed turbulence, but the velocity profile remains logarithmic. For dense submerged canopies, the drag-discontinuity at the top of the canopy generates a shear-layer, which contains canopy-scale vortices that control the exchange of mass and momentum between the canopy and the overflow. The canopy-scale vortices penetrate a finite distance into the canopy, δ_e, set by the canopy drag. This length-scale segregates the canopy into two regions: the upper canopy experiences energetic turbulent transport, controlled by canopy-scale vortices, while the lower canopy experiences diminished transport, associated with the smaller stem-scale turbulence. Flexible blades move in response to the canopy-scale vortices, called *monami*.

Introduction

Fresh- and saltwater vegetation provide a wide range of ecosystem services. Seagrasses are essential primary producers, forming the foundation for many food webs (Green & Short 2003). Seagrass meadows also damp waves, stabilize the seabed, shelter economically important fish, and enhance local water quality by filtering nutrients from the water. Based on nutrient cycling services alone, the global economic value of seagrass was estimated to be 3.8 trillion dollars per year by *Costanza et al.* (1997). Aquatic vegetation is also abundant in lowland rivers, where it provides habitat, alters light availability and temperature, and mediates concentrations of oxygen, carbon, and nutrients (Carpenter & Lodge 1986). Fresh- and saltwater wetlands provide habitat, improve water quality, and reduce coastal erosion (Mitsch & Gosselink 1986, Brampton 1992). Most of the services mentioned above are influenced by the flow within the vegetated regions.

The presence of vegetation alters the velocity field across several scales, ranging from individual branches and blades on a single plant, to the community of plants, called the meadow or canopy. The flow structure at the different scales is relevant to different processes. For example, the uptake of nutrients by an individual blade depends on the boundary layer on that blade, *i.e*. on the blade-scale flow (*e.g*. Koch 1994, Hurd 2000). Similarly, the capture of pollen is mediated by the flow structure generated around individual stigma (*e.g*. Ackerman 1997, 2000). In contrast, the flushing of larvae and pollen from a seagrass meadow or kelp forest depends on the flow structure at the canopy-scale (*e.g*. Jackson & Winant 1983, Gaylord et al. 2004).

Some aspects of canopy flow have been described in recent reviews. Monismith (2007) describes flow at branch- and canopy-scales in and around coral. Canopy-scale flow structure for terrestrial plant and urban canopies is described in Finnigan (2000) and Belcher (2012, this volume), and the mechanical interactions between wind and terrestrial plants are described by de Langre

(2008). To complement this rich literature, this review emphasizes conditions unique to aquatic vegetation. Specifically, unlike terrestrial canopies, aquatic canopies can occupy all or a large fraction of the flow depth, such that the dynamic impact of the canopy is felt over the entire flow domain. This review will focus on fully developed flow structure over and through long canopies. The adjustment of flow at the leading edge of a canopy is described in Belcher *et al*. (2003), Rominger & Nepf (2011), and Belcher (2012, this volume).

Geometric scales and momentum balance -

The canopy geometry is defined by the scale of individual stems and blades, and the number of these elements per bed area. If the canopy elements have a characteristic diameter or width, d, and the average spacing between elements is ΔS, then the frontal area per canopy volume is $a = d/\Delta S^2$. In terrestrial canopy literature, this is called the leaf area index (*e.g*. Kaimal & Finnegan 1994, p.79). A non-dimensional measure of the canopy density is the frontal area per bed area, λ_f, known as the roughness density (Wooding, Bradley & Marshall 1973). For canopy height h, and $z = 0$ at the bed,

$$\lambda_f = \int_{z=0}^{h} a dz = ah, \qquad (1)$$

with the right-most expression valid for vertically uniform a. The canopy density can also be described by the solid volume fraction occupied by the canopy elements, ϕ. If the individual elements approximate a circular cylinder, *e.g*. reed stems, then $\phi \approx (\pi/4)\, ad$. If the morphology is strap-like, *e.g*. seagrasses, with blade width d and thickness b, then $\phi = db/\Delta S^2 = ab$

Aquatic canopies exhibit a wide range of geometry. Marsh grasses are relatively sparse with

d = 0.1 cm to 1 cm, ϕ = 0.001 to 0.01, a = 0.01 to 0.07 cm^{-1} (based on Valiela et al. 1978; Leonard & Luther 1995, Lightbody & Nepf 2006). Mangroves are among the densest canopies, with ϕ as high as 0.45, mean trunk diameters of 4 to 9 cm, and a up to 0.2 cm^{-1} (Mazda et al. 1997; Furukawa et al. 1997). Seagrasses have a = 0.01 to 1 cm^{-1}, ϕ = 0.01 to 0.1 (Chandler et al. 1996, Luhar et al. 2010). Emergent plants tend to have rounded stems for higher stiffness, and submerged grasses tend to have a blade geometry in which the width (0.3 to 1 cm) is larger than the thickness (≈ 0.1 cm), in which case d is the blade width.

Within a canopy, flow is forced to move around each branch or blade, so that the velocity field is spatially heterogeneous at the scale of these elements. A double-averaging method is used to remove the element-scale spatial heterogeneity, in addition to the more common temporal averaging (Gray & Lee 1977; Raupach & Shaw 1982, and references therein). Let the coordinates x and z be parallel and normal to the local mean bed-slope, with z = 0 at the bed and positive away from the bed. The velocity vector $\vec{u} = (u,v,w)$ corresponds to the coordinates (x, y, z), respectively. The instantaneous velocity and pressure (p) fields are first decomposed into a time average (overbar) and deviations from the time-average (single prime). The time-averaged quantities are further decomposed into a spatial mean (angle bracket) and deviations from the spatial mean (double prime). The spatial averaging volume is thin in the vertical, to preserve vertical variation in canopy density, and large enough in the horizontal plane to include several stems (> ΔS).

Using the double-average method, the stream-wise momentum equation becomes

$$\frac{D\langle\overline{u}\rangle}{Dt} = g\sin\theta - \frac{1}{\rho}\frac{\partial\langle\overline{p}\rangle}{\partial x} - \frac{\partial}{\partial z}\left\langle\overline{u'w'}\right\rangle - \frac{\partial}{\partial z}\left\langle\overline{u}''\overline{w}''\right\rangle + \nu\frac{\partial^2\langle\overline{u}\rangle}{\partial z^2} - D_x \qquad (2)$$

(i) (ii) (iii)

Here, ρ is the water density, ν is the kinematic viscosity, θ is the bed slope, and g is the gravitational acceleration. Term (i) is the spatial-average of the Reynolds' stress. Term (ii), called the dispersive stress, is the momentum flux associated with spatial correlations in the time-averaged velocity field. Poggi et al. (2004b) have shown that the dispersive stress is less than 10% of the Reynolds stress (i) for $\lambda_f = ah > 0.1$. Term (iii) is the viscous stress associated with the spatial variation in $\langle \overline{u} \rangle$. The final term, D_x, is the spatially-averaged drag associated with the canopy elements, which is often represented by a quadratic drag law (*e.g.* Kaimal & Finnegan 1994, p. 95).

$$D_x = \frac{1}{2}\frac{C_D a}{1-\phi}\langle \overline{u} \rangle \left| \langle \overline{u} \rangle \right| \tag{3}$$

C_D is the canopy drag coefficient. Since the drag acts upon the fluid within the canopy, which occupies only (1-ϕ) of the total volume, the drag is divided by the factor (1-ϕ). The canopy-drag length-scale, L_c, is defined from the quadratic drag law, *i.e.* based on dimensional reasoning $D_x = \langle \overline{u} \rangle^2 / L_c$ (Belcher et al. 2003). From (3)

$$L_c = \frac{2(1-\phi)}{C_D a}. \tag{4}$$

This represents the length-scale over which the mean and turbulent flow components adjust to canopy drag. Since, most aquatic canopies have high porosity ($\phi < 0.1$), this scale is commonly approximated by $(C_D a)^{-1}$.

The drag coefficient, C_D, is affected by the canopy density, a, the element-Reynolds' number, $Re_d = < \bar{u} > d / \nu$, and the morphology of the individual canopy elements. A review of C_D's dependence on Reynolds' number and canopy density can be found in Tanino and Nepf (2008a) and Nepf (2011). A linear drag law provides a better fit for rigid vegetation under low element Reynolds number ($Re_d < 50$, Tanino et al. 2005). The Darcy-Forscheimer equation (*e.g.* Whitaker 1996) has also been used to describe drag in wetlands (Oldham & Sturman 2001) and coral canopies (Lowe et al. 2008). For flexible vegetation, the posture of the blade is affected by the flow speed, a phenomenon called reconfiguration. As velocity increases, the blades are pushed over into more streamlined positions, so that the drag force increases more slowly with increasing velocity than predicted by the quadratic drag law. The impact of a changing plant shape on drag force has been represented by altering the exponent in the drag law, while holding a, the frontal area, constant at the undisturbed (no flow) value, a_o. Specifically, the square power in (3) is replaced with a variable power $2+E$. The exponent E assumes values between 0 (rigid blade) and -2 (extremely flexible) depending on the type of vegetation (see e.g. Vogel, Ch.6, 1994, Alben et al. 2002, O'Hare et al. 2007, Sand-Jensen 2008, Gosselin *et al*. 2010, Green 2005). In practice, it is difficult to characterize the frontal area a for real plants, which has lead to contradictory results in the dependency of drag on velocity (*e.g*. see discussion of Sand-Jensen 2003 by Sukhodolov 2005, Green 2005, Statzner et al. 2006).

Emergent Canopies

An emergent canopy fills the entire water depth, H, and typically penetrates through the water surface. This type of canopy occurs in tidal marshes, kelp forests, and seagrass meadows during periods of low tide. Emergent canopies impose structure on both the mean and turbulent flow

over the entire water column. The canopy dissipates eddies with scales greater than the stem-scales of ΔS and d, while contributing additional turbulent energy at these stem scales (Figure 1). As a result, the dominant turbulent length-scale within a canopy is shifted downward from analogous conditions without vegetation. In an open channel (no vegetation) eddies scale with the water depth, H. In a channel with rigid vegetation, the integral length-scale of the turbulence, ℓ, is set by the smaller of the stem diameter, d, or the average distance to the nearest neighboring stem, S_n, regardless of water depth (Tanino & Nepf 2008b). In a square array of stems the average spacing and the average nearest neighbor spacing are the same, $\Delta S = S_n$, but in a random array, $S_n < \Delta S$. For $d \le S_n$, turbulence is generated within stem wakes (if the Reynolds number is sufficient), so that $\ell = d$. For $d > S_n$, turbulence is generated within the pore channels, so that $\ell = S_n$. These two regimes are depicted in Figure 2a. Even for solid volume fractions as low as 0.6% ($a = 0.01\text{cm}^{-1}$) the production of turbulence by the canopy exceeds the production by bed shear over most of the flow depth (Nepf *et al.* 1997, Burke & Stolzenbach 1983, Lopez & Garcia 1998). Therefore, turbulence level *cannot* be predicted from the bed-friction velocity, as it is for open-channel flow. Instead, it is a function of the canopy drag, as described below.

Vortex generation by stem wakes and/or in pore channels drains energy from the mean flow (expressed as canopy drag) and feeds it into the turbulent kinetic energy. If this conversion is 100% efficient, then the rate at which turbulent energy is produced, P_W, is equal to the rate at which mean flow energy is extracted, *i.e*. the rate of work done by the flow against canopy drag (*e.g*. Raupach and Shaw 1982).

$$P_w = \frac{1}{2} C_D a \langle \bar{u} \rangle^3 \tag{5}$$

In fact, only the form drag is converted into turbulent kinetic energy. The viscous drag component is immediately dissipated to heat. For stiff canopies, *i.e*. most emergent canopies, and $Re_d > \approx 200$, the majority of the drag is form drag, and (5) is a reasonable approximation (Tanino & Nepf 2008 a, b). In contrast, Nikora & Nikora (2007) suggest that for flexible canopies, which are typically submerged, the drag is predominantly viscous, and (5) would be an overestimate of stem-scale turbulence production. The relative contributions of viscous drag and form drag depend on the morphology and alignment (streamlined vs. bluff) of the blades and stems within the canopy.

Within a homogenous emergent canopy, transport terms are negligible, and the wake production (5) is balanced by viscous dissipation, ε, *i.e*. $P_W = \varepsilon$. In addition, for turbulence kinetic energy, k, the dissipation rate within the canopy has the scale (Tennekes & Lumley 1972),

$$\varepsilon \sim \left\langle \bar{k} \right\rangle^{3/2} \ell^{-1} \tag{6}$$

Equating (5) and (6), the turbulence intensity in the canopy is,

$$\frac{\sqrt{\left\langle \bar{k} \right\rangle}}{\left\langle \bar{u} \right\rangle} \sim \left(C_D a \ell \right)^{1/3}. \tag{7}$$

As describe above, the turbulence length scale, ℓ, is set by the smaller of the stem diameter, d, and nearest-neighbor stem spacing, S_n. In a canopy of low solid volume fraction, or specifically $S_n > d$, the turbulence intensity increases rapidly with increasing canopy density (Figure 2b), because $\ell = d$, and thus $a\ell \approx d^2/S_n^2$ in (7). In a canopy of high solid volume fraction, $S_n < d$, the turbulence intensity increases more slowly, because $\ell = S_n$, and thus $a\ell \approx d/S_n$ in (7).

Mean Velocity Profile

Within an emergent canopy, the momentum equation (2) will generally simplify to a balance between potential forcing (associated with hydrostatic pressure or bed slope) and canopy drag. First, viscous stress, $\nu \partial^2 \langle \bar{u} \rangle / \partial z^2$, is negligible compared to vegetative drag over most of the depth, excluding a thin layer near the bed of a scale comparable to the stem diameter, d (Nepf & Koch 1999). Second, as discussed above, the eddy length-scale is small compared to the water depth, which limits the turbulence flux of momentum, *i.e.* the turbulence stresses are typically negligible. For example, from numerical experiments the eddy scales are 1-3% of the water depth, and turbulent stresses are only 2% of the total drag for $aH = 0.1$ (Burke & Stolzenbach 1983). Similar ratios have measured in model emergent canopies (Nepf & Vivoni 2000). A notable exception occurs near the surface, as wind-generated stress can sometimes play a role in the momentum balance (Jenter & Duff 1999). Third, we assume that dispersive fluxes are negligible because the canopy density is commonly above the threshold $ah > 0.1$ suggested by Poggi et al (2004b). For steady, uniform flow, the momentum equation then reduces to

$$g\left(\frac{\partial H}{\partial x} + \sin\theta\right) = -\frac{1}{2}\frac{C_D a}{1-\phi}\langle \bar{u} \rangle \left|\langle \bar{u} \rangle\right| = -\frac{\langle \bar{u} \rangle \left|\langle \bar{u} \rangle\right|}{L_c}. \tag{8}$$

The hydrostatic pressure and potential gradients that drive the flow (left-hand side) are not functions of the vertical coordinate, z. The right-hand side must then also be independent of z, so that the velocity varies inversely with the frontal area, a, and in proportion to the canopy-drag length scale, L_c. For plants with a distinct basal stem, this produces a velocity maximum close to the bed, because

1 *a* is reduced below the level at which branching begins (Figure 1). A near-bed velocity maximum is
2 often observed in the marsh grass *Spartina alterniflora* (Leonard & Luther 1995, Leonard & Croft
3 2006). In contrast, the more vine-like *Atriplex portuloides* has leaves (and thus $C_D a$) that are more
4 evenly distributed over depth, and the resulting velocity profile is uniform over depth (Leonard &
5 Reed 2002).

6 Equation 8 implies that the velocity profile within an emergent canopy has a self-similar
7 form. When the velocity is normalized by its value at an arbitrary reference depth, denoted by
8 subscript *ref*, the normalized profiles collapse together, regardless of the absolute magnitude of the
9 current. The shape of the normalized profile depends on the vertical distribution of L_c.
10

11 $$\frac{\langle \overline{u} \rangle}{\langle \overline{u} \rangle_{ref}} = \sqrt{\frac{L_c}{L_{c-ref}}} \approx \sqrt{\frac{(C_D a)_{ref}}{(C_D a)}} \qquad (9)$$

12

13 The right-most approximation holds in most salt- and fresh-water wetlands canopies, for which the
14 canopy solid volume fraction is small ($\phi < 0.1$), so that $(1-\phi) \approx 1$. A self-similar velocity structure
15 was confirmed by measurements in a coastal marsh (Lightbody & Nepf 2006) and in the freshwater
16 wetlands of the Everglades (Huang et al 2008). The normalization in (9) provides an important tool
17 for extrapolating a full velocity profile from records at a single vertical position.

18 An interesting non-linear behavior emerges when we compare flow conditions under
19 different canopy density, but the same potential and/or pressure gradient. To include the no canopy
20 limit, *i.e*. bare-bed, the bed resistance must be included in the momentum balance. Figure 2c and 2d
21 depict the change in velocity and turbulent kinetic energy, respectively, relative to bare-bed
22 conditions, with the later denoted by subscript *b*. The details of this comparison are given in Nepf

(1999). Because the vegetation offers additional resistance, the velocity within the canopy is always less than that over a bare bed, and the velocity ratio, $< \overline{u} > / u_b$, decreases as the vegetation density increases (Figure 2c). Changes in turbulent kinetic energy with increasing vegetation density reflect the competing effects the reduced velocity and the additional turbulence production in stem wakes (7). These opposing tendencies produce a non-linear response in which the turbulence levels initially increase with increasing canopy density, but decrease as *a* increases further (Figure 2d). This non-linear response was predicted numerically for flow through emergent vegetation (Burke & Stolzenbach 1983) and within submerged roughness elements (Eckman 1990). It has been observed in flume studies of flow through real stems of *Zostera Marina* (Gambi *et al*. 1990). The enhanced turbulence levels in sparse canopies have important implications for canopy ecology. An increase in turbulence, particularly element-scale turbulence, could benefit vegetation by augmenting nutrient uptake and/or gas exchange (Anderson & Charters 1982), and similarly enhance uptake by microbes living on plant surfaces (*e.g*. Gantzer *et al*. 1991). Significant contributions to the turbulence intensity from stem-scale turbulence has also been observed in beds of channel macrophytes (Naden *et al*. 2006).

It is commonly expected that dense patches of vegetation, because they damp flow and turbulence, are associated with muddification, an increase in fine particles and organic content of the underlying sediment relative to adjacent bare bed conditions. Recently, van Katwijk et al (2010) observed that sparse patches of vegetation are associated with sandification, a decrease in fine particles and organic matter, and they attribute this to higher levels of turbulence within the sparse patch, relative to adjacent bare regions. A transition from a tendency for sandification (elevated turbulence) to a tendency for muddification (diminished turbulence intensity) with increasing canopy density is consistent with the non-linear model shown in Figure 2d.

Submerged Canopies

The velocity within a submerged canopy has a range of behavior depending on the relative depth of submergence, defined as the ratio of flow depth, H, to canopy height, h. The flow within the canopy is driven by the turbulent stress at the top of the canopy as well as by the gradients of pressure and gravitational potential (bed slope). The relative importance of these driving forces varies with the depth of submergence (Nepf & Vivoni 2000).

$$\frac{turbulent\ stress}{pressure\ gradient} \sim \frac{H}{h} - 1 \qquad (10)$$

Three classes of canopy flow can be defined from (10): deeply submerged or unconfined ($H/h > 10$); shallow submergence ($H/h < 5$); and emergent ($H/h = 1$). A great deal is known about unconfined canopy flow based on work in terrestrial canopies (*e.g*. Raupach *et al*. 1996, Finnegan 2000, Belcher 2012). When unconfined, the flow within a canopy is driven by the turbulent stress at the top of the canopy, *i.e*. by the vertical turbulent transport of momentum from the overflow, with negligible contribution from pressure gradients. The terrestrial canopy model can be applied to aquatic canopies that are deeply submerged. However, due to the limitation of light penetration, most submerged aquatic canopies occur in the range of shallow submergence $H/h < 5$ (*e.g*. Duarte 1991, Chambers and Kalff 1985), for which both turbulent stress and potential gradients are important in driving flow in the canopy. For emergent conditions ($H/h = 1$) flow is driven by the potential gradients, as described in the previous section.

For a submerged canopy, there are two limits of behavior, depending on the relative importance of the bed shear and the canopy drag. If canopy drag is small compared to bed drag, then the velocity follows a turbulent boundary layer profile, with the vegetation contributing to the bed roughness (Figure 3c, sparse canopy). If the canopy drag is large compared to the bed stress, the discontinuity in drag that occurs at the top of the canopy ($z = h$) generates a region of shear resembling a free-shear-layer with an inflection point near the top of the canopy (Figure 3de, dense canopy). From scaling arguments, Belcher et al (2003) predict that the transition between the sparse and dense regimes occurs at the roughness density $\lambda_f = ah = 0.1$. Numerical simulations in Coceal & Belcher (2004, Figure 4 of that paper) suggest that the transition occurs at $L_c/h = 5$, which corresponded to $\lambda_f = 0.15$, for their parameter set ($C_D = 2$, $\phi = 0.25$). Based on measured velocity profiles in aquatic systems (Nepf et al 2007, and references therein), the profile exhibits a boundary-layer form with no inflection point if $C_D ah < 0.04$. A pronounced inflection point appears at the top of the canopy for $C_D ah > 0.1$. Since $C_D \approx 1$ in most of the studies considered, these limits are consistent with the scaling and numerical estimates given above.

In this paper we focus on the dense canopy condition ($ah > 0.1$). For these canopies, Raupach et al (1996) demonstrated a similarity between canopy-shear-layers and free-shear-layers. In a free-shear-layer the velocity profile contains an inflection point, which triggers a flow instability that, in turn, leads to the generation of Kelvin-Helmoltz vortices (*e.g.* Brown & Roshko 1974, Winant & Browand 1974). These structures dominate the transfer of momentum between the high-speed and low-speed streams, and their size sets the length-scale of the shear-layer. For dense submerged canopies ($ah > 0.1$), the momentum absorption by the canopy is sufficient to produce an inflection point in the velocity profile, which, as in free-shear-layers, leads to the generation of K-H vortices (Figure 3de). These vortices are called canopy-scale turbulence, to distinguish it from the

much-larger boundary-layer turbulence, which may form above a deeply submerged or unconfined canopy, and the much smaller stem-scale turbulence.

Over a deeply submerged (or terrestrial) canopy ($H/h > 10$), the canopy-scale vortices are highly three-dimensional due to their interaction with larger boundary-layer turbulence, which stretches the canopy-scale vortices, enhancing secondary instabilities (Fitzmaurice et al. 2004, Finningan et al 2009). However, with shallow submergence ($H/h <= 5$), which is common in aquatic systems, larger-scale boundary-layer turbulence is not present, and the canopy-scale vortices dominate the turbulence field, both within and above the canopy (Ghisalberti & Nepf 2005, 2009). For shallow submergence the canopy-scale turbulence is also more coherent (less three-dimensional) than that observed with deeply submerged (or terrestrial) conditions. However, in both cases the canopy-scale vortices dominate the vertical transport at the canopy interface (*e.g.* Gao et al. 1989, Finnigan 2000, Ghisalberti & Nepf 2002).

In a free-shear-layer, the vortices grow continually downstream, predominantly through vortex pairing (Winant & Browand 1974). In canopy-shear-layers, however, the vortices reach a fixed scale and a fixed penetration into the canopy (δ_e in Figure 3de) at a short distance from the canopy's leading edge (Ghisalberti & Nepf 2004). Based on measurements with a flexible model of the seagrass *Zostera marina* ($a = 5.7$ m^{-1}), a fixed shear-layer scale is reached at a distance of $10h$ from the leading edge of the meadow (Ghisalberti 2000). The fixed vortex and shear-layer scale is reached when the shear-production that feeds energy into the canopy-scale vortices is balanced by dissipation by canopy drag. This energy balance predicts the following length-scale, which has been verified with laboratory observations (Nepf et al. 2007).

$$\delta_e = \frac{0.23 \pm 0.6}{C_D a} \qquad (11)$$

Recall that $C_D ah \geq 0.1$ is required to produce shear-layer vortices, so that (11) applies only to those canopies. In the range $C_D ah = 0.1$ to 0.23, the shear-layer vortices penetrate to the bed, $\delta_e = h$, creating a highly turbulent condition over the entire canopy height (Figure 3d). At higher values of $C_D ah$ the canopy-scale vortices do not penetrate to the bed, $\delta_e < h$ (Figure 3e).

The scaling $\delta_e \sim a^{-1}$ has been observed in flows near porous layers over a wide range of physical scales, spanning from granular beds to terrestrial forests and urban canopies (Ghisalberti, 2009). However, the scale relation must break down when $(C_D a)^{-1}$ approaches the scale of the canopy elements, d, because a is only defined as an average over multiple elements. For rigid cylinders, when $(C_D a)^{-1}$is less than $2d$, the penetration scale transitions to a constant $\delta_e \approx 2d$ (White & Nepf 2007). The depth of submergence, H/h, can also affect the penetration length-scale. For $H/h < 2$, δ_e is diminished from (11), as interaction with the water surface diminishes the strength and scale of the vortices (Nepf & Vivoni 2000, Okamoto & Nezu 2009).

The penetration length, δ_e, segregates the canopy into an upper layer of strong turbulence and rapid renewal and a lower layer of weak turbulence and slow renewal (Nepf & Vivoni 2000). Flushing of the upper canopy is enhanced by the canopy-scale vortices that penetrate this region (Figure 3e). In contrast, turbulence in the lower canopy ($z < h-\delta_e$) is generated in stem wakes and has significantly smaller scale, set by the stem diameters and spacing. Canopies for which $\delta_e/h < 1$ (Figure 3e) shield the bed from strong turbulence and turbulent stress. Because turbulence near the bed plays a role in resuspension, these dense canopies are expected to reduce resuspension and trap sediment. Consistent with this, Moore (2004) observed that resuspension within a seagrass meadow was reduced, relative to bare-bed conditions, only when the above ground biomass per unit area was greater than 100 g/m^2 (dry mass). This biomass corresponds to $ah = 0.4$ (Luhar et al. 2008). Using

$C_D \approx 1$, this canopy density is consistent with the transition implied by (11). Note that the transition in near-bed turbulence and resuspension does not occur abruptly at $C_D ah = 0.23$, but gradually with increasing $C_D ah$ above this value, as the canopy-scale vortices are progressively pushed further from the bed. Because of the reduced near-bed turbulence, dense canopies can promote sediment retention. In sandy regions, that tend to be nutrient poor, the preferential retention of fines and organic material, *i.e.* muddification, enhances the supply of nutrient to the canopy, so that dense canopies provide a positive feedback to canopy health in sandy regions. In contrast, in regions with muddy substrate, which is more susceptible to anoxia, sparse meadows ($C_D ah \leq 0.23$) may be more successful, because the enhanced near-bed turbulence removes fines, leading to a sandier substrate that is less prone to anoxia.

Flexible Canopies and Monami

Under some conditions, the canopy-scale vortices produce sufficient instantaneous drag to overcome the buoyancy and rigidity of individual blades. The passage of the travelling vortices then causes a local depression in the canopy, which travels along the canopy interface, in synch with the travelling vortices (Figure 4a). This progressive waving of canopy blades is called *monami* (Ackerman & Okubo 1993). It has been observed to occur extensively in the field (*e.g.* Fonseca & Kenworthy 1987, Ackerman & Okubo 1993, Grizzle *et al*. 1996). The frequency of the *monami* matches the frequency of vortex passage, which is given by instability theory (Ikeda & Kanazawa 1996, Ghisalberti & Nepf 2002). However, if the instantaneous drag associated with the canopy-scale vortices is not sufficient to depress individual blades, the *monami* will not occur, even though the canopy-scale vortices are present.

To understand the connection between the canopy-shear-layer vortices and the *monami*, it is

useful to consider the differences between the free-shear-layer and canopy-shear-layer. Free-shear-layer vortices are symmetric around the inflection point (z_i), and their translation speed, U_v, matches the velocity at the inflection point, U_i. Because these vortices rotate faster than they translate, the lower region of the layer experiences a negative velocity perturbation as a vortex passes (*e.g.* Dimotakis *et al*. 1981, Ho *et al*. 1991). In a canopy-shear-layer the inflection point corresponds with the top of the canopy ($z_i \approx h$), so that the velocity at the inflection point is $U_i = U_h = <\overline{u}>_h$. However, due to the canopy drag, the vortices are displaced upward, relative to the inflection point. As a result, the translation speed of the vortex is higher than the velocity at the inflection point, *i.e.* $U_v > U_i = U_h$ (Ikeda and Kanazawa 1996). The velocity ratio U_v/U_h increases with increasing depth of submergence (H/h), up to $U_v/U_h = 1.8$ observed at $H/h = 4.5$ (Ghisalberti & Nepf 2002). In terrestrial canopies U_v/U_h is also 1.8 (Finnigan 1979), suggesting that this is the asymptotic value for unconfined canopies. Further, the canopy drag causes the vortices to rotate more slowly than vortices formed in a free-shear-layer of comparable shear-strength. The translation speed of the vortex is sufficiently large compared to its rotation that as the front of the vortex passes a strong sweep ($u > 0$, $w < 0$) invades the canopy (Ghisalberti & Nepf 2002). The monami is generated as the sweep deflects the canopy forward and downward. The connection between the velocity field and the plant motion is described in Ghisalberti & Nepf (2006) and Okamoto & Nezu (2009).

The flexibility of the canopy and the presence of *monami* affect the turbulent exchange between the canopy and the overflow. This can be seen in the profiles of Reynolds' stress, normalized by the square of the velocity difference (ΔU) between the canopy and overflow, which is a measure of momentum exchange efficiency. The two profiles shown in Figure 4b are measured with the same flexible canopy ($a \approx 0.052$ cm^{-1}, and $ah = 1$ when erect, described in Ghisalberti & Nepf 2005). The vertical axis is dimensional to emphasize the vertical shift associated with the

greater deflection of the canopy under the higher flow condition. In the weaker flow case (U_h = 1.7 cms^{-1}, orange symbols) canopy-scale vortices are produced, but are too weak to deflect the blades, and no *monami* occurs. In the stronger flow case (U_h = 7.9 cms^{-1}, green), the canopy deflection is larger (smaller h), and the canopy-scale vortices are strong enough to trigger *monami*. The *monami* excursion amplitude is noted in the figure. The combination of deflection and *monami* allows the turbulent flux to penetrate closer to the bed, which leads to greater in-canopy flow speed (see also Ghisalberti & Nepf 2009).

While *monami* allows for a deeper penetration of stress, the momentum transfer is less efficient. For example, the maximum normalized stress is $\left\langle \overline{u'w'} \right\rangle \Big/ \left(\Delta U\right)^2 = 0.013$ for the stationary canopy (orange, w/o *monami*) but only 0.008 with *monami* is present (green, Figure 4b). A rigid canopy produces even more efficient exchange, with a peak normalized-stress of 0.017 (Ghisalberti & Nepf 2005). The diminished exchange efficiency occurs because the vortices are smaller and weaker in the presence of *monami*, and also weaker above a flexible canopy compared to a rigid canopy of similar geometry (see detailed discussion in Ghisalberti & Nepf 2006).

Mean Velocity Profile

Sufficiently far above a submerged canopy ($z > 2h$), the velocity profile is logarithmic (*see* Kaimal & Finnigan 1994, and reference therein).

$$< \overline{u} >= \frac{u_*}{\kappa} ln\left(\frac{z - z_m}{z_o}\right) \qquad (12)$$

with $\kappa = 0.4$ (von Karman constant). The horizontal-average (angled bracket) is not strictly needed above the canopy, but is retained for consistency with the equations within the canopy. The friction velocity, u_*, is related to the Reynolds' stress at the top of the canopy, $u_*^2 = <\overline{u'w'}>_h$. The parameters z_m and z_o are the displacement and roughness heights, respectively, both of which depend on the canopy roughness density, ah. Based on studies with both model and real vegetation, a simple estimate for friction velocity is $u_* = (gS(H - h))^{0.5}$, with $S = \partial H/\partial x + \sin\theta$ (Murphy *et al*. 2007). If the vegetation is flexible, then h is the mean deflected height of the canopy (Jarvela 2005). However, if the depth of submergence is small, compared to the displacement height, the following estimator is more accurate, $u_* = (gS(H - z_m))^{0.5}$ (Nepf & Vivoni 2000).

Recall that the penetration length-scale, δ_e, describes the distance over which turbulent stress penetrates the canopy from above. Similarly, the displacement height is the centroid of momentum penetration into the canopy (Thom 1971). This similarity suggests the physically intuitive scaling,

$$\frac{z_m}{h} \approx 1 - \frac{1}{2}\frac{\delta_e}{h} = 1 - \frac{0.1}{C_D a h}, \qquad (13)$$

which has been confirmed for $ah \approx 0.2$ to 3 (Luhar et al 2008). For $ah >\approx 1$, the displacement thickness tends towards $z_m \approx h$, indicating that essentially the entire canopy is cut-off from the overflow. In addition, z_m goes to zero at $ah = 0.1$. When $z_m = 0$, the velocity profile has no inflection point (Figure 3c), consistent with the observation $ah > 0.1$ is required to produce an inflection point in measured velocity profiles (Figure 3de).

The dependency of the roughness height, z_o, on canopy density, ah, differs significantly above and below the threshold of $ah = 0.1$ (*e.g*. Raupach *et al*. 1980, MacDonald *et al*. 1998,

Jimenez 2004, Luhar *et al*. 2008). In the sparse canopy range ($ah < 0.1$), the roughness height increases with increasing ah. In sparse canopies the flow penetrates the full canopy, so that z_o is proportional to the drag imparted by the full canopy, $C_D ah$, *i.e*. $z_o/h \sim C_D ah$. In contrast, for dense canopies ($ah > 0.1$), the roughness height decreases with increasing ah. The effective height of the canopy, as seen by the overflow, is the penetration scale, δ_e. The roughness height depends on this effective height, rather than the canopy height, so that $z_o \sim \delta_e \sim a^{-1}$. For example, data summarized in Luhar et al (2008) suggest that for $ah > 0.1$, $z_o = (0.04 \pm 0.02)\, a^{-1}$.

The logarithmic profile form is based on equilibrium turbulence, such that dissipation and production are locally in balance (*e.g*. Tennekes & Lumley 1990). Largely because of the vertical transport provided by the shear-layer structures, this condition is not met for some distance above the canopy, called the roughness sub-layer. For very shallow submergence, $H/h \leq 1.5$, the roughness sub-layer extends to the surface, and a logarithmic structure is not observed above the canopy.

The flow within a submerged canopy is driven by a combination of the turbulent, dispersive and viscous (usually negligible) stresses generated by the overflow, as well as the potential gradient associated with the hydrostatic pressure gradient and the bed slope. Below the penetration of turbulent and dispersive stress ($z < h-\delta_e$), conservation of linear momentum reduces to a balance between potential gradients and the sum of the canopy and the bed drag. Assuming that the canopy drag is much larger than bed drag, this balance yields the following mean velocity.

$$\langle \bar{u} \rangle = U_1 = \sqrt{\frac{2g(\partial H / \partial x + \sin\theta)}{C_D a}} \qquad (14)$$

This is the same momentum balance observed for emergent canopies. So, again, if the canopy

density, a, or drag coefficient C_D are functions of z, the velocity will vary inversely, *i.e.* velocity will be highest where $C_D a$ is lowest.

In the upper canopy ($h-\delta_e < z < h$) flow is driven by both potential gradients and turbulent stress. The stress-driven component is derived by simplifying the moment equation (2) to a balance of canopy drag and turbulent stress, and modeling the turbulent stress with a mixing length model, $\left\langle \overline{u'w'} \right\rangle = \ell_m^2 (\partial < \overline{u} > / \partial z)^2$ (*e.g.* Inoue 1963, Cionco 1965). This yields the exponential velocity profile observed in terrestrial canopies. In aquatic canopies, the potential-driven component is also important in the upper canopy. Combining the stress-driven and potential-driven components, the upper canopy velocity profile is,

$$\left\langle \overline{u} \right\rangle = U_1 + (U_h - U_1) exp(-K_u (h - z)), \qquad (15)$$

with $U_h = \left\langle \overline{u} \right\rangle$ at the top of the canopy, and constant $K_u = \beta / \ell_m$, with $\beta = u_*/U_h$. It is physically-intuitive that the mixing length should be related to the penetration of shear-layer vortices into the canopy, *i.e.* $\ell_m \sim \delta_e \sim (C_D a)^{-1}$. Harmon and Finnigan (2007) suggest $\ell_m = 2\beta^3 (C_D a)^{-1}$, or $K_u = C_D a/(2\beta^2)$. For rigid canopies in water, $\beta = 0.24 \pm 0.02$ (S.E., data in Ghisalberti & Nepf 2005), which predicts $K_u = (8.7 \pm 1.4)\, C_D a$. This predicted value agrees with the observed decay scale constant, $K_u = (9 \pm 2) C_D a$, extracted from measured velocity profiles in Ghisalberti (2005). In the dense canopy limit, β has no dependence on canopy density (Ghisalberti & Nepf 2005), but it declines as the transition to the sparse canopy limit ($ah < 0.1$) is approached, *i.e.* as the canopy-scale vortices diminish and eventually disappear (Poggi et al 2004a). Flexible canopies display a lower value, $\beta = 0.17 \pm 0.01$ (Ghisalberti & Nepf 2005), consistent with the less efficient momentum transfer noted in Figure 4. Belcher et al (2003) propose the alternative $K_u = (2 l_m^2 L_c)^{-1/3}$, with the

approximation $l_m \sim h$. However, the mixing length within the canopy may be better represented by the vortex penetration, *i.e.* $l_m \sim L_c \sim (C_D a)^{-1}$, which then also yields $K_u \sim L_c^{-1} \sim C_D a$.

To model the full velocity profile, *i.e.* both within and above the bed, researchers have combined the models for above-canopy and in-canopy profiles by matching the velocity at the top of the canopy (*e.g.* Abdelrhman 2003, Carollo *et al.* 2002). While this ignores the roughness sub-layer, for practical purposes the resulting profile is reasonably accurate. First, the velocity profile above the meadow ($z > h$) is estimated from the logarithmic profile (12). The logarithmic profile provides the velocity at the top of the meadow, U_h, which is used with (14) and (15) to predict the velocity within the meadows ($z < h$). An example is given in Figure 5 using data from Ghisalberti (2005). The input parameters are the water depth (H = 46.7 cm), the meadow height (h = 13.9 cm), the surface slope ($S = 2.5 \times 10^{-5}$), the canopy density ($a = 0.034$ cm^{-1}), and the measured drag coefficient, $C_D = 0.77$. The measured and predicted profiles agree within uncertainty, except approaching the free-surface, where the measured profile tends toward $\partial u/\partial z = 0$ to meet the no-stress condition at the surface that is not represented in the log-profile. Other models for the complete velocity profile in regions with submerged aquatic vegetation have utilized different turbulence closure schemes (*e.g.* Shimizu & Tsujimoto 1994, Lopez & Garcia 2001, Poggi et al 2004a, Defina & Bixio 2005), and some reflect the bending response of flexible vegetation (e.g. Abdelrhman 2007, Dikstra & Uittenbogaard 2010)

Mass Transport in Vegetated Flow

Conservation of mass is described by the transport equation,

$$\frac{\partial C}{\partial t} + \vec{u} \cdot \nabla C = D_m \nabla^2 C, \qquad (16)$$

with D_m the molecular diffusion. Applying the double-average method described above, and assuming there are no sources or sinks, this becomes,

$$\frac{\partial\langle\overline{C}\rangle}{\partial t}+\langle\overline{u}_j\rangle\frac{\partial\langle\overline{C}\rangle}{\partial x_j}=-\frac{1}{(1-\phi)}\frac{\partial}{\partial x_j}(1-\phi)\left\{\langle\overline{u_j'C'}\rangle+\langle\overline{u}_j''\overline{C}''\rangle-D_m\left\langle\frac{\overline{\partial C}}{\partial x_j}\right\rangle\right\}, \qquad (17)$$

with $(x, y, z) = (x_1, x_2, x_3)$. The first term on the right-hand side represents dispersion associated with turbulent fluctuations, *i.e*. turbulent diffusion. The second term on the right represents dispersion associated with spatial-heterogeneity in the time-mean velocity field, *e.g*. the dispersion associated with flow path turtuosity. The last term is flux due to molecular diffusion, which in general is negligible compared to the first two. Laboratory measurements in rigid canopies indicate that, over time-scales greater than turbulent time-scales, and spatial-scales much greater ΔS and d, these three terms produce Fickian transport, *i.e*. the right hand-side reduces to $D_j\left(\partial^2\langle\overline{C}\rangle/\partial x_j\right)$, with dispersion coefficient D_j (White & Nepf 2003, Tanino & Nepf 2008b).

Turbulent Diffusion and Mechanical Dispersion in an Emergent Canopy

For solid volume fraction $\phi < 0.1$, turbulent diffusion is the dominant component of D within the canopy (Tanino & Nepf 2008b). The velocity scale controlling turbulent diffusion is the mean velocity, U_1, given by (8) and (14). As discussed above, the turbulence length scale may be set by the stem scale (if $d \le S_n$), or by the stem spacing S_n, for $d > S_n$ (Figure 2a). Experimental studies confirm $D \sim U_1 d$ for $\phi <\approx 0.1$, and support the simple scaling,

$$D = 0.2\, U_1 d \tag{18}$$

(Lightbody & Nepf 2006, Tanino & Nepf 2008b). For denser canopies, specifically when $S_n < d$, the contribution to D from turbulent diffusion declines rapidly, as the length-scale of turbulence declines (Figure 2a). For $\phi >\approx 0.1$, the dispersion due to the spatial-heterogeneity in the velocity field (also called mechanical dispersion) becomes important, and it dominates for $\phi > 0.15$. In addition, in the absence of turbulence, *e.g.* $Re_d < 100$, mechanical dispersion is the main contributor to dispersion across all stem densities. The following formulation is consistent with data across all stem densities for $Re_d < 100$, and for $\phi > 0.15$ for all Reynolds number (Nepf et al. 1997, Serra et al. 2004, Nepf 2004, Tanino & Nepf 2008b),

$$\frac{D}{U_1 d} = ad \approx \phi \tag{19}$$

Tanino & Nepf (2008b) describe a more comprehensive model that smoothly spans the two regimes described by (18) and (19).

Turbulent Diffusion within and Above a Submerged Canopy

Because the canopy drag restricts the penetration of the canopy-scale vortices, a submerged canopy is segregated into two zones characterized by distinct turbulence scales. The canopy-scale vortices are excluded from the lower canopy ($z < h\text{-}\delta_e$), and as a result the mechanisms of dispersion resemble those described above for emergent canopies. In contrast, transport in the upper canopy ($z > h\text{-}\delta_e$) is dominated by the canopy-scale turbulence, so that the turbulent diffusivity scales on the

size of the canopy-scale vortices and the velocity difference, ΔU, between the canopy and the overflow, *e.g.* shown in Figure 4. The canopy-scale vortices grow to a size comparable to the shear-layer thickness t_{ml}. These scales also apply above a canopy with shallow submergence ($H/h < 5$), because the canopy-shear-layer extends over most of the flow depth (Ghisalberti & Nepf 2005, Ghisalberti & Nepf 2009). Based on experiments with rigid canopies,

$$D \approx 0.02\,\Delta U\, t_{ml} \qquad (20)$$

over the entire shear-layer, *i.e.* both above and within the canopy (Figure 11 in Ghisalberti & Nepf 2005). Generally, $t_{ml} \sim h$, so (20) can be estimated from the canopy height, h, and the velocity difference, ΔU. The turbulent diffusivity has a peak at the top of the canopy, with $D\,(z = h) \approx 0.032 \Delta U\, t_{ml}$. As in a free-shear layer, the turbulent diffusivity is higher than the turbulent viscosity (ν_t). The turbulent Schmidt number ($S_t = \nu_t / D_t$) has a mean of 0.5 within the canopy-shear layer, similar to other free shear layers, and a minimum of 0.3 at the top of the canopy, so that mass is mixed across the canopy–water interface three times more rapidly than is momentum (Ghisalberti & Nepf 2005, and references therein). For reference, in a neutral boundary layer $S_t \approx 1$ (*e.g.*, Kaimal & Finnigan 1994, *p.* 125). The lower value of S_t within a canopy shear-layer can be explained by the numerical results discussed in Fitzmaurice *et al* (2004). Ensemble averages of the velocity and pressure fields show that a region of high dynamic pressure is generated when a sweep encounters the canopy. While sweep events carry momentum and scalar downward via identical motions, the momentum transport is offset by high pressure generated at the canopy boundary, depressing the turbulent Schmidt number.

Summary

Aquatic vegetation significantly alters the mean and turbulent flow field. Within emergent canopies, the turbulent length-scales are set by the stem diameter and spacing, and the mean flow is determined by the distribution of canopy frontal area. Sparse submerged canopies ($ah < 0.1$) enhance bed roughness and near-bed turbulence, but the velocity profile remains logarithmic. In contrast, dense submerged canopies ($ah > 0.1$) transfer the velocity profile to a mixing layer. These canopies generate two distinct scales of turbulence: canopy-scale turbulence generated by flow instability at the top of the canopy, and stem-scale turbulence generated within the canopy. The canopy-scale turbulence penetrates into the canopy only over a length-scale dependent on the canopy drag, $\delta_e \sim (C_D a)^{-1}$. This length-scale determines both the displacement thickness (z_m) for the logarithmic velocity profile above the canopy, as well as the decay of stress-driven flow within the canopy. Further, δ_e separates a dense canopy into two regions of distinct transport. The upper canopy ($z > h-\delta_e$) experiences energetic vertical transport and high levels of turbulent diffusion, controlled by canopy-scale vortices. The lower canopy ($z < h-\delta_e$) experiences significantly slower transport, associated with the smaller element-scale turbulence.

Acknowledgements-

The author is grateful for the insight and creativity of current and former students who contributed to this research, M. Ghisalberti, E. Murphy, B. White, A. Lightbody, Y. Tanino, M. Luhar, and J. Rominger, and especially for the editorial comments provided by M. Luhar and J. Rominger. Some of this material is based upon work supported by the National Science Foundation under Grant No. EAR0309188, EAR 0125056, EAR 0738352 and OCE 0751358. Any opinions, conclusions or

recommendations expressed in this material are those of the author(s) and do not necessarily reflect the views of the National Science Foundation.

Literature Cited

Abdelrhman M. 2003. Effect of eelgrass Zostera marina canopies on flow and transport. *Mar. Ecol.-Prog. Ser*. 248:67-83

Abdelrhman M. 2007. Modeling coupling between eelgrass Zostera marina and water flow. *Mar. Ecol. Prog. Ser*. 338:81–96, doi:10.3354/meps338081

Ackerman JD, Okubo A. 1993. Reduced mixing in a marine macrophyte canopy. *Fun. Ecol*. 7:305-09

Ackerman JD. 1997. Submarine pollination in the marine angiosperm *Zostera marina*. *Amer. J. Botany* 84(8):1110-19

Ackerman JD. 2000. Abiotic pollen and pollination: ecological, functional, and evolutionary perspectives. *Plant Syst. Evol*. 222:167-85

Alben S, Shelley M, Zhang J. 2002. Drag reduction through self-similar bending of a flexible body. *Nature* 420:479-81

Anderson S, Charters A. 1984. A fluid dynamics study of seawater flow through *Gelidium nudifrons*. *Limnol Ocean*. 27(3):399-412

Belcher S, Jerram N, Hunt J. 2003. Adjustment of a turbulent boundary layer to a canopy of roughness elements. *J. Fluid Mech*. 488: 369-98

Belcher S. 2012. Canopy Flows. *Ann. Rev. of Fluid Mechanics*, 44, (this volume)

Brampton AH. 1992. Engineering significance of British saltmarshes. *In* Saltmarshes: Morphodynamics, Conservation, and Engineering Significance, ed. JRL Allen, K Pye, Cambridge University Press, p. 115–122

Brown G, Roshko A. 1974. On density effects and large structure in turbulent mixing layers. *J. Fluid Mech*. 64:775-816

Burke R, Stolzenbach K. 1983. Free surface flow through salt marsh grass. MIT-Sea Grant Technical Report MITSG 83-16, Cambridge, MA

Carollo F, Ferro V, Termini D. 2002. Flow velocity measurements in vegetated channels. *J. Hydraul. Eng*.-ASCE, 128(7), doi: 10.1061/0733-9429

Carpenter SR, Lodge DM. 1986. Effects of submersed macrophytes on ecosystem processes. *Aquatic Botany* 26:341-70

Chambers PA, Kalff J. 1985. Depth distribution and biomass of submersed aquatic macrophyte communities in relation to Secchi depth. *Can. J. Fish. Aquat. Sci*. 42:701–09

Chandler M, Colarusso P, Buchsbaum R. 1996. A study of eelgrass beds in Boston Harbor and northern Massachusetts bays. Office of Res. and Devel., US EPA, Narragansett, RI

Cionco R. 1965. A mathematical model for air flow in a vegetation canopy. *J. Appl. Met*. 4:517-22

Coceal O, Belcher S. 2004. A canopy model of mean winds through urban areas. *Q.J.R. Meteorol. Soc*., 130:1349-72

Costanza R, d'Arge R, de Groot R, Farber S, Grasso M, et a. 1997. The value of the world's ecosystem services and natural capital. *Nature* 387:253-60

de Langre E. 2008. Effects of wind on plants. *Ann. Rev. Fluid. Mech*., 40:141-68, doi:10.1146/annurev.fluid.40.111406.102135

Defina A, Bixio A. 2005. Mean flow and turbulence in vegetated open channel flow. *Water. Res. Res.* 41, W07006, doi:10.1029/2004WR003475

Dijkstra J, Uittenbogaard R. 2010. Modeling the interaction between flow and highly flexible aquatic vegetation. *Water. Res. Res*. 46, W12547, doi:10.1029/2010WR009246

Dimotakis P, Debussy F, Koochesfahani M. 1981. Particle streak velocity field measurements in a two-dimensional mixing layer. *Phys. Fluids* 24(6*)*:995-99

Duarte CM. 1991. Seagrass depth limits. *Aquat. Bot.* 40:363–77

Eckman J. 1990. A model of passive settlement by planktonic larvae onto bottoms of differing roughness. *Limnol. Oceanogr*. 35:887-901

Finnigan J. 1979. Turbulence in waving wheat: I. Mean statistics and honami. *Bound.-Layer Meteorol.* 16:181-211

Finnigan J. 2000. Turbulence in plant canopies. *Ann. Rev. Fluid Mech*. 32:519-71

Finnigan J, Shaw R, Patton E. 2009. Turbulence structure above a vegetation canopy. *J. Fluid Mech*. 637:387-424

Fitzmaurice L, Shaw R, Paw U KT, Patton E. 2004. Three-dimensional scalar microfronts in a large-eddy simulation of vegetation canopy flow. *Bound.-Layer Met*. 112:107–27

Fonseca M, Kenworthy W. 1987. Effects of current on photosynthesis and distribution of seagrasses. *Aquat. Bot*. 27:59–78

Furukawa K, Wolanski E, Mueller H. 1997. Currents and sediment transport in mangrove forests. *Est., Coast. Shelf Sci.* 44:301-10

Gambi M, Nowell A, Jumars P. 1990. Flume observations on flow dynamics in *Zostera marina* (eelgrass) beds. *Mar. Ecol. Prog. Ser.* 61:159-69

Gantzer C, Rittmann B, Herricks E. 1991. Effect of long-term water velocity chnages on streambed biofilm activity. *Wat. Res*. 25:15-20

Gao W, Shaw R, Paw U KT. 1989. Observation of organized structure in turbulent flow within and above a forest canopy. *Bound.-Layer Meteorol.* 47:349–77

Gaylord B, Reed D, Washburn L, Raimondi P. 2004. Physical-biological coupling in spore dispersal of kelp forest macroalgae. *J. Mar. Syst*. 49:19-39

Ghisalberti M. 2000. *Mixing Layers and coherent structures in vegetated aquatic flows*. MS Thesis. Massachusetts Instititute of Technology. 126 pp.

Ghisalberti M. 2005. Momentum and Scalar Transport in Vegetated Shear Flows. PhD Thesis. Massachusetts Institute of Technology. 119 pp.

Ghisalberti M. 2009. Obstructed shear flows: similarities across systems and scales. *J. Fluid Mech*. 641:51-61

Ghisalberti M, Nepf H. 2002. Mixing layers and coherent structures in vegetated aquatic flow. *J. Geophys. Res.*, 107(C2), 10.1029/2001JC000871

Ghisalberti M, Nepf H. 2004. The limited growth of vegetated shear -layers. *Water Res. Res.* 40, W07502, doi:10.1029/2003WR002776

Ghisalberti M, Nepf H. 2005. Mass Transfer in Vegetated Shear Flows. *Env. Fluid Mech*. 5(6): 527-51, doi10.1007/s10652-005-0419-1

Ghisalberti M, Nepf H. 2006. The structure of the shear layer over rigid and flexible canopies. *Env. Fluid Mech*. 6(3):277-301, doi10.1007/s10652-006-0002-4

Ghisalberti M, Nepf H. 2009. Shallow flows over a permeable medium: the hydrodynamics of submerged aquatic canopies. *Transp. Porous Media.* 78:385-402, doi:10.1007/s11242-009-9434-x

Gosselin F, deLangre E, and Machado-Almeida B. 2010. Drag reduction of flexible plates by reconfiguration, *J. Fluid Mech*. 650:319-41

Green EP, Short FT. 2003. *World Atlas of Seagrasses*, Univ. California Press, 310 pp.

Green J. 2005. Further comment on drag and reconfiguration of macrophytes. *Freshwater. Biol*. 50:2162-66

Gray WG, Lee PCY. 1977. On the theorems for local volume averaging of multiphase systems. *Inter. J. Multiphase Flow.* 3(4):333-40

Grizzle R, Short F, Newell C, Hoven H, Kindblom L. 1996. Hydrodynamically induced synchronous waving of seagrasses: monami and its possible effects on larval mussel settlement. *J. Exp. Mar. Biol. Ecol*. 206:165–77

Harman I, Finnigan J. 2007. A simple unified theory for flow in the canopy and roughness sublayer. *Bound.-Lay. Met*., 123:339-63, doi10.1007/s10546-006-9145-6

Ho C-M, Zohar Y, Foss J, Buell J. 1991. Phase decorrelation of coherent structures in a free shear layer. *J. Fluid Mech.* 230:319-37

Huang Y-H, Saiers J, Harvey J, Noe G, Mylon S. 2008. Advection, dispersion, and filtration of fine particles within emergent vegetation of the Florida Everglades. *Water. Res. Res*. 44, W04408, doi:10.1029/2007WR006290

Hurd CL. 2000. Water motion, marine macroalgal physiology, and production. J. Phycol. 36:453-72

Ikeda S, Kanazawa M. 1996. Three-dimensional organized vortices above flexible water plants, *J. Hydraul. Eng.* 122(11):634-40

Inoue E. 1963. On the turbulent structure of airflow within crop canopies. J. Met. Soc. Japan 49:121–24

Jackson G, Winant C. 1983. Effect of a kelp forest on coastal currents. *Cont. Shelf. Res*. 2(1):75-80

Jarvela J. 2005. Effect of submerged flexible vegetation on flow structure and resistance, *J. Hydrology 307*:233-41

Jenter H, Duff M. 1999. Locally-forced wind effects on shallow waters with emergent vegetation, in Proceedings of the 3rd International Symposium on Ecohydraulics, Salt Lake City, Utah, July 13-16, CD-ROM

Jimenez J. 2004. Turbulent flows over rough walls. *Ann. Rev. Fluid Mech.* 36:173-96

Kaimal J, Finnigan J. 1994. *Atmospheric Boundary Layer Flows: Their Structure and Measurement*. Oxford University Press, Oxford, 289 pp.

Koch EW. 1994. Hydrodynamics, diffusion-boundary layers and photosynthesis of the seagrasses, *Thalassia testudinum* and *Cymodocea nodosa*. *Marine Biology*, 118:767-76

Leonard L, Luther M. 1995. Flow hydrodynamics in tidal marsh canopies. *Limnol. Oceanogr*. 40: 1474-84

Leonard L, Reed D. 2002. Hydrodynamics and sediment transport through tidal marsh canopies. *J. Coast. Res*. 36:459-69

Leonard L, Croft A. 2006. The effect of standing biomass on flow velocity and turbulence in *Spartina alterniflora* canopies. *Coast. Shelf. Sci*. 69:325-36

Lightbody A, Nepf H. 2006. Prediction of velocity profiles and longitudinal dispersion in emergent salt marsh vegetation. *Limnol. Ocean.* 51(1):218-28

Lopez F, Garcia M. 1998. Open-channel flow through simulated vegetation: suspended sediment transport modeling. *Water Res. Res*. 34(9):2341-52

Lopez F, Garcia M. 2001. Mean flow and turbulence structure of open-channel flow through non-emergent vegetation. *J. Hydraul. Res*. 127:392-402

Lowe R, Shavit U, Falter J, Koseff J, Monismith S. 2008. Modeling flow in coral communities with and without waves: A synthesis of porous media and canopy flow approaches. *Limnol. Ocean*. 53(6):2668-80

Luhar M, Rominger J, Nepf H. 2008. Interaction between flow, transport and vegetation spatial structure. *Env. Fluid Mech.* 8(5-6):423-39

Luhar M, Coutu S, Infantes E, Fox S, Nepf H. 2010. Wave induced velocities inside a model seagrass bed. *J.Geophys. Res.* 115*, C12005,* doi:10.1029/2010JC006345

Macdonald R, Griffiths R, Hall, D. 1998. An improved method for the estimation of surface

roughness of obstacle arrays. *Atmos*. *Environ*. 32(11):1857-64

Mazda, Y, Wolanksi E, King B, Sase A, Ohtsuka D, Magi M. 1997. Drag forces due to vegetation in mangrove swamps. *Mangr. Salt Marsh*, 1:193–99

Mitsch WJ, Gosselink JG. 1986. *Wetlands*. 2nd Ed. Van Nostrand Reinhold, 712pp

Monismith S. 2007. Hydrodynamics of corals. *Ann. Rev. Fluid. Mech*. 39:37-55

Moore KA. 2004. Influence of seagrasses on water quality in shallow regions of the lower Chesapeake Bay, *J. Coast. Res.*, 20 (Special Issue):162-78

Murphy E, Ghisalberti M, Nepf H. 2007. Model and laboratory study of dispersion in flows with submerged vegetation, *Water Res. Res*., 43, W05438, doi:10.1029/2006WR005229

Naden P, Rameshwaran P, Mountford O, Robertson C. 2006. The influence of macrophyte growth, typical of eutrophic conditions, on river flow velocities and turbulence production. *Hydrol. Proc.* 20:3915-38

Nepf H. 1999. Drag, turbulence, and diffusion in flow through emergent vegetation. *Water Res. Res.* 35:479-89

Nepf H. 2004. Vegetated flow dynamics. In *Ecogeomorphology of Tidal Marshes*. ed. S Fagherazzi, M Marani, L Blum. Coastal and Estuarine Monograph Series. AGU. doi:10.1029/59CE09

Nepf H. 2012. Flow over and through biota. In: Treatise on Estuarine and Coastal Science. ed. E Wolanski, D McLusky, Elsevier Inc., San Diego

Nepf H, Ghisalberti M, White B, Murphy E. 2007. Retention time and dispersion associated with submerged aquatic canopies, *Water Res. Res*., 43, W04422, doi:10.1029/2006WR005362

Nepf H, Koch E. 1999. Vertical secondary flows in submersed plant-like arrays. *Limnol*. *Oceanogr*. 44(4):1072-80

Nepf H, Sullivan J, Zavistoski R. 1997. A model for diffusion within an emergent plant canopy. *Limnol. Oceanogr.* 42(8):85-95

Nepf H, Vivoni E. 2000. Flow structure in depth-limited, vegetated flow. *J. Geophys. Res.* 105(28):547-57

Nikora N, Nikora V. 2007. A viscous drag concept for flow resistance in vegetated channels. Proceedings of the 32nd IAHR Congress, Venice, 1-6 July, CD-ROM

O'Hare M, Hutchinson K, Clarke R. 2007. The drag and reconfiguration experienced by five macrophytes from a lowland river. *Aquatic Botany*, 86:253-59

Okamoto T, Nezu I. 2009. Turbulence structure and monami phenomena in flexible vegetated open-channel flows. *J. Hydraulic Res*., 47(6):798-810

Oldham C, Sturman J. 2001. The effect of emergent vegetation on convective flushing in shallow wetlands. *Limnol. Ocean*. 46:1486-93

Poggi D, Porporato A, Ridolfi L, Albertson J, Katul G. 2004a. The effect of vegetation density on canopy sub-layer turbulence. *Bound. Lay. Met.* 111:565-87

Poggi D, Katul G, Albertson J, 2004b. A note on the contribution of dispersive fluxes to momentum transfer within canopies. *Bound. Lay. Met.* 111:615-21

Raupach M, Thom A, Edwards I. 1980. A wind-tunnel study of turbulent flow close to regularly arrayed rough surfaces. *Bound. Lay. Met.* 18:373-97

Raupach M, Shaw R. 1982. Averaging procedures for flow within vegetation canopies. *Bound. Lay. Met. 22*:79-90

Raupach M, Finnigan J, Brunet Y. 1996. Coherent eddies and turbulence in vegetation canopies: The mixing-layer analogy. *Bound. Lay. Met*. 60:375-95

Rominger R, Nepf H. 2011. Flow adjustment to and interior flow within a rectangular porous obstruction. In revision for *J. Fluid Mech*.

Sand-Jensen K. 2003. Drag and reconfiguration of freshwater macrophytes. *Fresh. Bio*. 48:271-83

Sand-Jensen K. 2008. Drag forces on common plant species in temperate streams: consquences of morphology, velocity, and biomass. *Hydrobiologia*, 610:307-19

Serra T, Fernando HJS, Rodriquez R. 2004. Effects of emergent vegetation on lateral diffusion in wetlands. *Water Research*, 38:139-47

Shimizu Y, Tsujimoto T. 1994. Numerical analysis of turbulent open-channel flow over a vegetation layer using a k-ε turbulence model. *J. Hydrosci. Hydraul. Eng*. 11:57-67

Statzner B, Lamouroux N, Nikora V, Sagnes P. 2006. The debate about drag and reconfiguration of freshwater macrophytes: comparing results obtained by three recently discussed approaches. *Freshwater Biol*. 51:2173-83

Sukhodolov A. 2005. Comment on drag and reconfiguration of macrophytes. *Freshwater Biol*. 50:194-95

Tanino Y, Nepf H, Kulis P. 2005. Gravity currents in aquatic canopies. *Water Res. Res*., 41, W12402, doi:10.1029/2005WR004216

Tanino Y, Nepf H. 2008a. Laboratory investigation on mean drag in a random array of rigid, emergent cylinders. *J. of Hydr. Eng.* 134(1):34-41, doi:10.1061/(ASCE)0733-9429(2008)134:1(34)

Tanino Y, Nepf H. 2008b. Lateral dispersion in random cylinder arrays at high Reynolds number. *J. Fluid Mech.* 600:339-71

Tennekes H, Lumley J. 1972. *A First Course in Turbulence*. MIT Press, Cambridge, MA, 300 pp.

Thom A. 1971. Momentum absorption by vegetation. *Q. J. R. Meteorol. Soc*. 97:414-28

Townsend, AA. 1976. The Structure of Turbulent Shear Flow, 2nd ed., Cambridge University Press, 444 pp.

van Katwijk M, Bos A, Hermus D, Suykerbuyk W. 2010. Sediment modification by seagrass beds: muddification and sandification induced by plant cover and environmental conditions. Est.,

Coastal, Shelf Sci. doi:10.1016/j.ecss.2010.06.008

Valiela I, Teal J, Deuser W. 1978. The nature of growth forms in the salt marsh grass *Spartina alterniflora*. *American Naturalist*, 112:461-70

Vogel S. 1994. *Life in Moving Fluid* 2nd Ed., Princeton University Press, Princeton, NJ, 484 pp.

Whitaker S. 1996. The Forchheimer equation: A theoretical development. *Trans. Porous Media.* 25:27-61

White B, Nepf H. 2003. Scalar transport in random cylinder arrays at moderate Reynolds number. *J. Fluid Mech*. 487:43-79

White B, Nepf H. 2007. Shear instability and coherent structures in a flow adjacent to a porous layer, *J. Fluid Mech*. 593:1-32

Winant C, Browand F. 1974. Vortex pairing, the mechanism of turbulent mixing-layer growth at moderate Reynolds number. *J. Fluid Mech*. 63:237-55

Wooding R, Bradley E, Marshall J. 1973. Drag due to regular arrays of roughness elements. *Bound. Lay. Met*. 5:285-308

Figure 1. Emergent canopy of marsh grass, with vertical profiles of leaf area index, *a*, and longitudinal velocity, $< \overline{u} >$. The velocity profile varies inversely with *a*, creating a velocity maximum close to the bed, below the level at which branching begins.

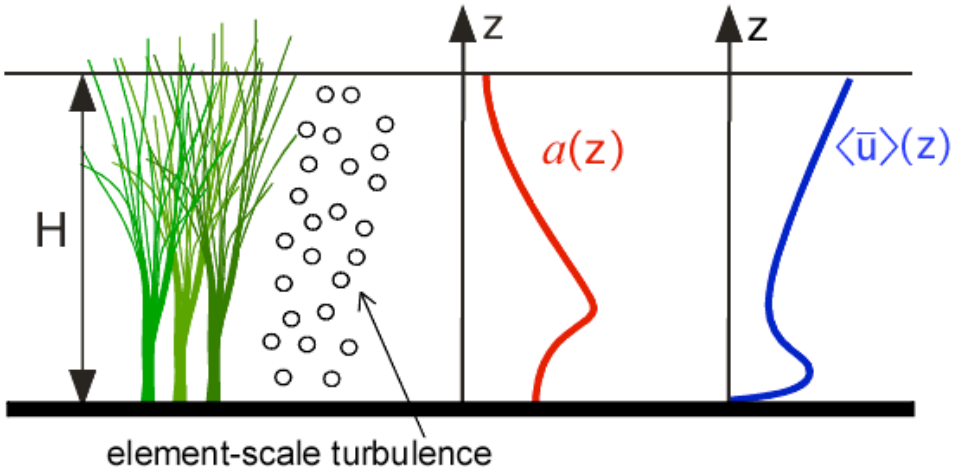

Figure 2. Changes in flow properties with increasing stem density. (a) The integral scale of turbulence, ℓ, is set by the smaller of two canopy scales: the stem diameter, d, and the nearest-neighbor stem spacing, S_n. If $d < S_n$, $\ell = d$. If $d > S_n$, $\ell = S_n$. (b) The turbulence intensity, given by (7), depends on the integral length-scale of the turbulence. If $d < S_n$, the turbulence intensity increases rapidly with increasing stem density, because $a\ell \approx d^2/S_n^2$. If $d > S_n$, the turbulence intensity increases more slowly, as $a\ell \approx d/S_n$. Changes in (c) velocity and (d) turbulent kinetic energy, with increasing stem density, shown relative to values for a bare-bed (sub-script b) with the same forcing. Based on Fig. 10 in Nepf 2012, reproduced with the kind permission of Elsevier Press.

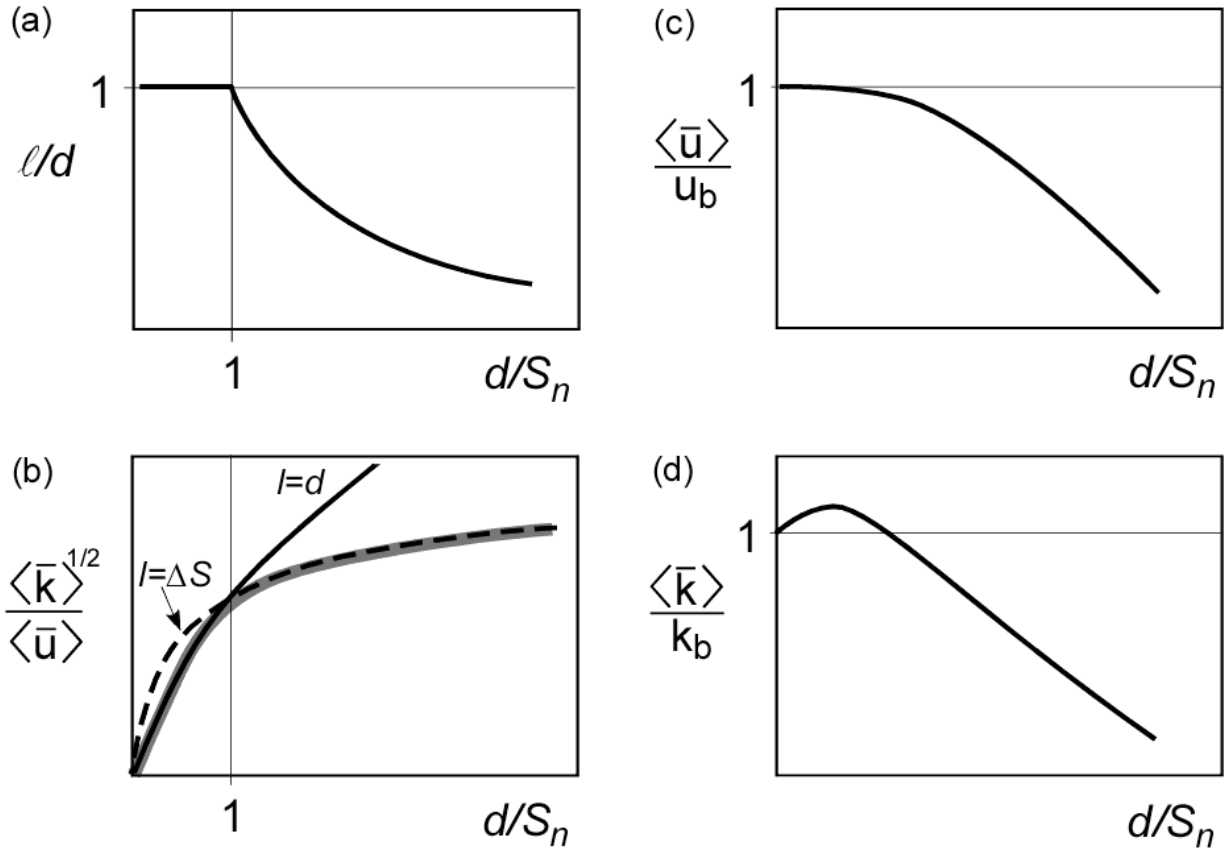

Figure 3 a) seagrass *Cymodocea nodosa* at low stem density b) seagrass *Posidonia oceanica at* high stem density. Photos by Eduardo Infantes Oanes. Vertical profiles of longitudinal velocity and dominant turbulence scales for (c) sparse canopy ($ah << 0.1$), (d) transitional canopy ($ah \approx 0.1$) and (e) dense canopy ($ah > 0.1$). h is the submerged canopy height. For $ah \approx > 0.1$, a region of strong shear at the top of the canopy generates canopy-scale turbulence. Element-scale (stem-scale) turbulence is generated within the canopy.

a)

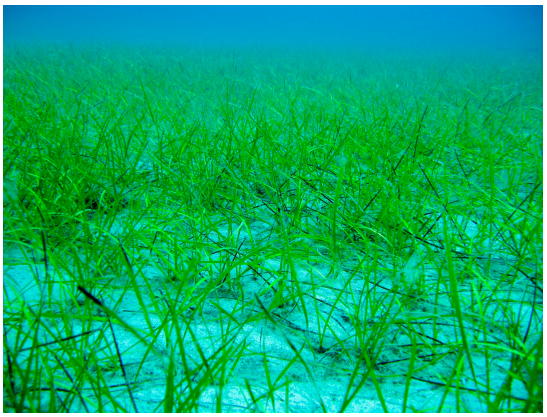

b)

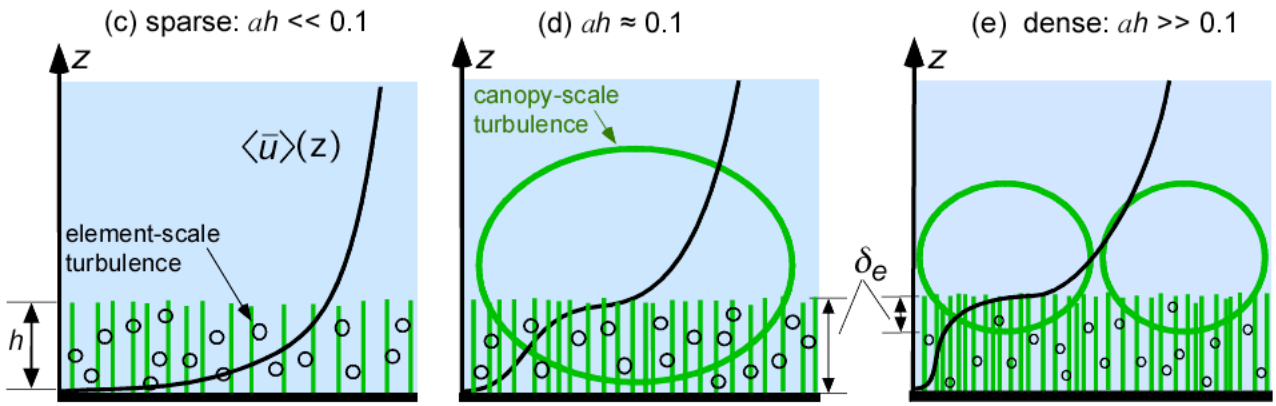

Figure 4. a) For dense submerged canopies ($ah > 0.1$), the drag discontinuity at the top of the canopy generates a region of shear resembling a free-shear-layer, which in turn generates canopy-scale vortices by Kelvin-Helmholtz instability. The passage these canopy-scale vortices over the canopy may generate a progressive waving of the canopy that is called *monami* (green canopy). If the shear-layer vortices are too weak, the canopy will bend, but not wave (orange canopy). b) Profiles of normalized turbulent stress in and above a flexible canopy for two flow conditions, based on data from Ghisalberti and Nepf (2006). With the weaker current, no *monami* occurs (orange dots). With a stronger current, *monami* is produced (green dots). The vertical excursion of the canopy interface associated with the *monami* is shown with the dashed double-arrow. Under the stronger current (green dots), the individual blades are deflected further, reducing the mean canopy height (h), relative to the condition with the weaker current (orange dots).

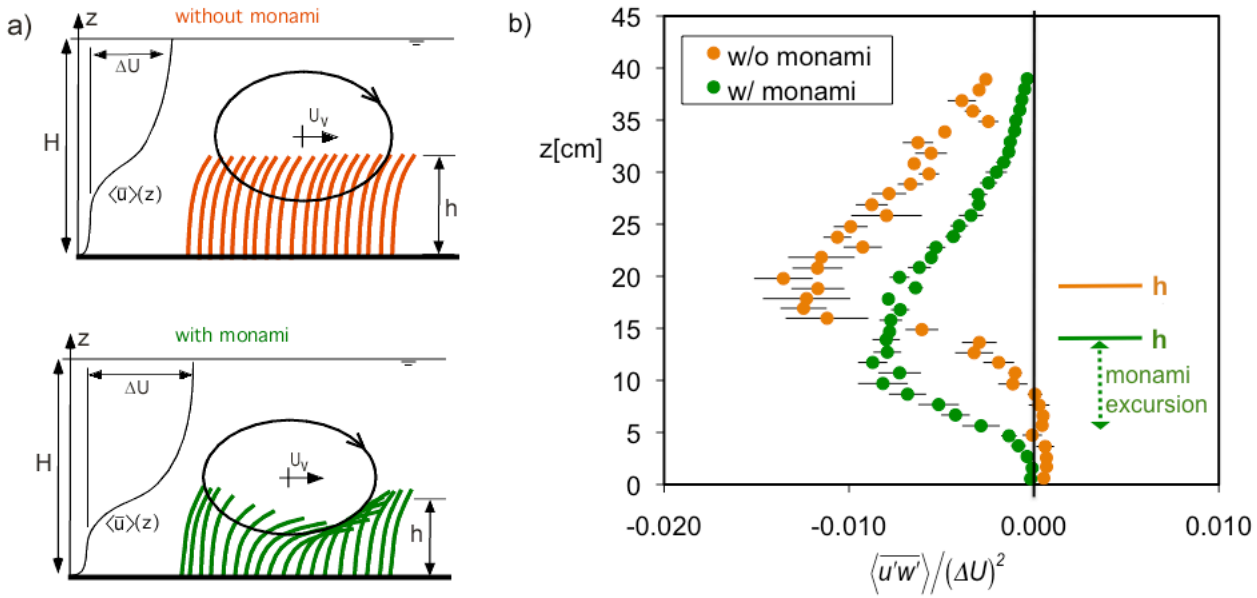

Figure 5. Measured velocity (dots) from Ghisalberti (2005). Predicted velocity (solid line) with confidence limits (dashed lines); $H = 46.7$ cm, $h = 13.9$ cm, $S = 2.5 \times 10^{-5}$, $a = 0.034$ cm^{-1}, $C_D = 0.77$ (measured). Above the meadow, the velocity is predicted from the logarithmic profile (12), with $u_* = (gS(H-h))^{1/2}$, $z_m = h-(1/2)\delta_e$ (13), and $z_o = (0.04 \pm 0.02)a^{-1}$, as given in text. Inside the meadow the velocity is predicted from (14) and (15), with U_h taken from logarithmic fit.